

European Journal of Inorganic Chemistry

Supporting Information

Chiral Emissive Lanthanide Complexes from Enantiopure [6]Helicene-bis(pyrazolyl)-pyridine Ligands

Alexandre Abhervé,* Maurizio Mastropasqua Talamo, Nicolas Vanthuyne, Francesco Zinna,
Lorenzo Di Bari, Maxime Grasser, Boris Le Guennic,* and Narcis Avarvari*

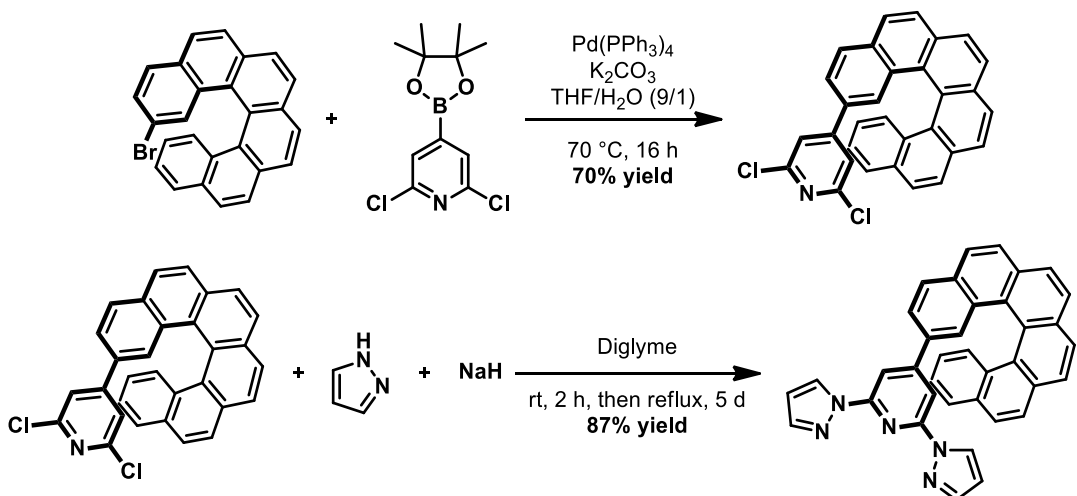
Index

Experimental section	2
Chiral HPLC	6
Crystallographic data of the ligands	10
Synthesis and characterization of the complexes	13
UV-Vis / CD spectroscopy of the complexes	17
CPL of the complexes	19
Computational part	20

Experimental section

Materials and methods. The precursors $[\text{Eu}(\text{tta})_3(\text{H}_2\text{O})_2]$, $[\text{Yb}(\text{tta})_3(\text{H}_2\text{O})_2]^1$ and 2-bromo[6]helicene² were prepared as previously reported in the literature. All other materials and solvents were commercially available and used without further purification. Nuclear magnetic resonance spectra were recorded on a Bruker Avance DRX 300 spectrometer (operating at 300 MHz for ¹H and 75 MHz for ¹³C). Chemical shifts are expressed in parts per million (ppm) downfield from external TMS. MALDI-TOF MS spectra were recorded on Bruker Biflex-IIITM apparatus, equipped with a 337 nm N₂ laser. Elemental analyses were recorded using Flash 2000 Fisher Scientific Thermo Electron analyser. UV-Vis absorption spectra were recorded using a Shimadzu UV 1800 spectrometer in 10^{-5} M CH₂Cl₂ solutions. Excitation and emission spectra were recorded using a RF-6000 spectrometer in 10^{-6} M CH₂Cl₂ solutions. CD spectra were recorded on a JASCO J-1500 spectrometer at 20°C. CPL measurements were carried out with a home-made spectrofluoropolarimeter,³ mounting a Hamamatsu R-376 for visible measurements and a Hamamatsu R-316 for NIR ones.⁴ The samples concentration was around $1 \cdot 10^{-1}$ M. A 365 nm LED was used as the excitation source, employing a 90°. Luminescence dissymmetry factors (g_{lum}) were calculated as $2(I_L - I_R) / (I_L + I_R)$, where I_L and I_R are left and right circularly polarized components of the emission. The spectra are the average of 8 accumulations each.

Synthesis of 1-bpp[6]helicene. Racemic 1-bpp[6]helicene was prepared as previously reported.⁵ The precursor dichloropyridine-[6]helicene was obtained by a Suzuki coupling between 2-bromo[6]helicene and 2,6-dichloropyridine-4-boronic acid pinacol ester. After reaction with sodium pyrazolate, 1-bpp[6]helicene was obtained as a racemic mixture. Both **6M** and **6P** enantiomers were separated by semi-preparative chiral HPLC on Chiralpak IE (250 x 10 mm).



¹H NMR (300 MHz, CDCl₃) : δ 8.52 (d, *J* = 2.5 Hz, 2H, H1-H4), 8.15 (d, *J* = 8.6 Hz, 1H), 8.16 (m, 1H), 8.04 – 7.93 (m, 8H), 7.87 (d, *J* = 1.1 Hz, 2H), 7.65 (ddd, *J* = 8.4, 7.8, 1.7 Hz, 2H, H3-H6), 7.31 (s, 2H, H7-H8), 7.20 (ddd, *J* = 8.1, 6.9, 1.2 Hz, 1H), 6.72 (ddd, *J* = 8.3, 6.9, 1.3 Hz, 1H), 6.51 (dd, *J* = 2.5, 1.7 Hz, 2H, H2-H5). ¹³C NMR (75 MHz, CDCl₃) : δ 154.3, 150.3, 142.1, 134.3, 133.2, 132.4, 132.4, 131.8, 131.7, 130.2, 129.6, 128.7, 128.7, 128.2, 127.9, 127.7, 127.7, 127.5, 127.2, 127.0, 125.8, 124.8, 124.1, 107.9, 107.6. MALDI: 537.

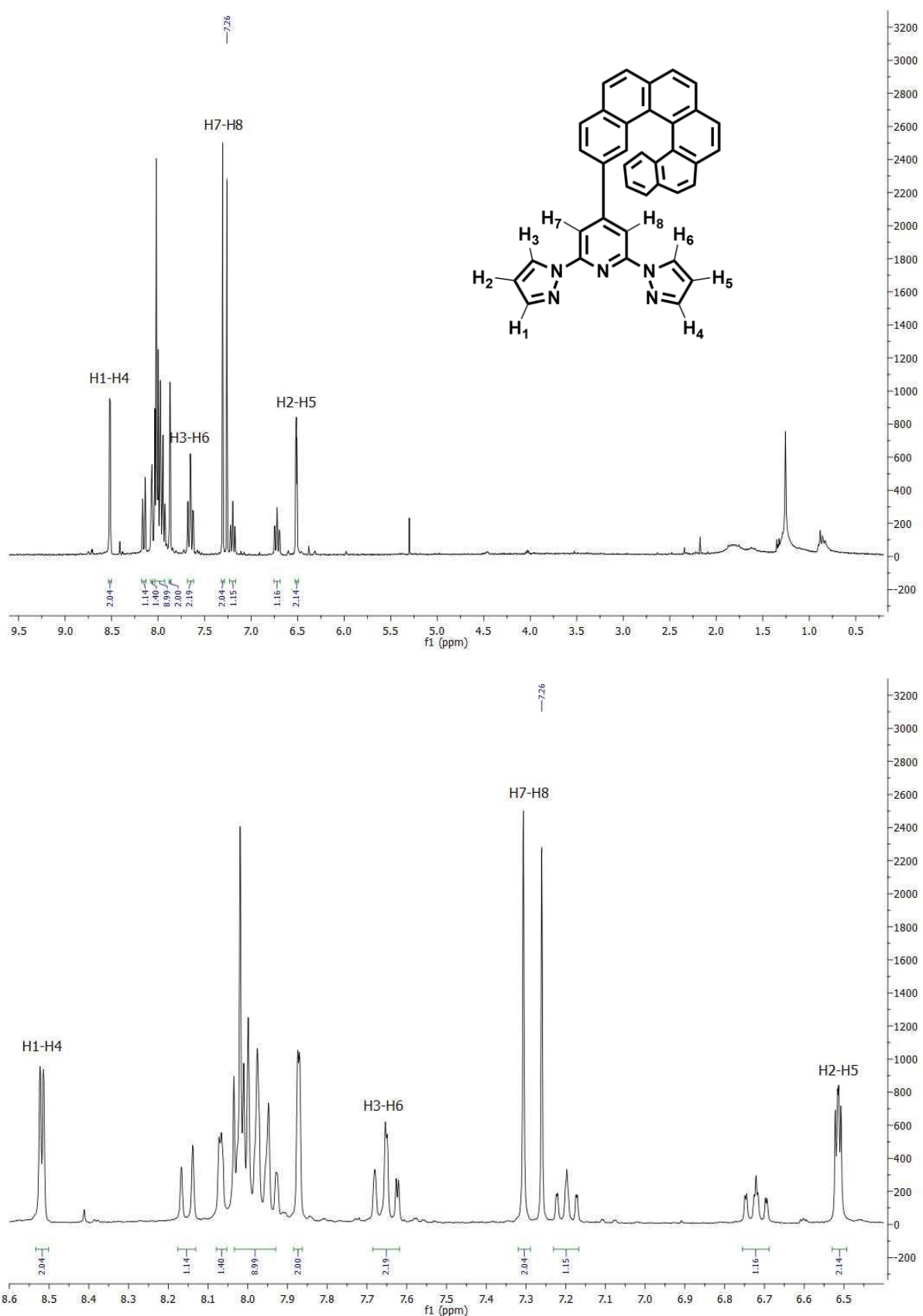


Figure S1. ^1H NMR spectra of 1-bpp[6]helicene in the full range (top) and in the aromatic region (bottom).

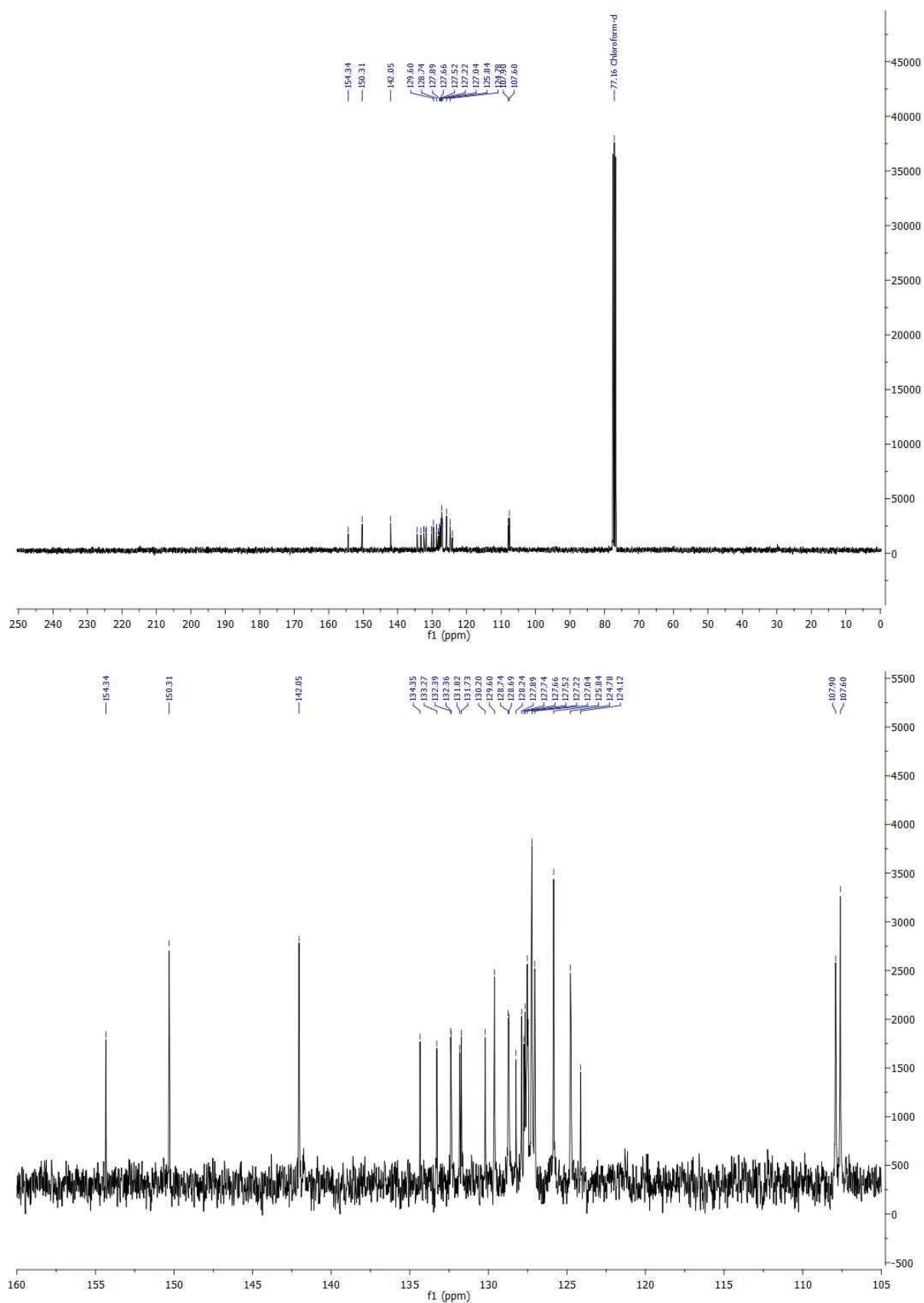


Figure S2. ^{13}C NMR spectra of 1-bpp[6]helicene in the full range (top) and in the aromatic region (bottom).

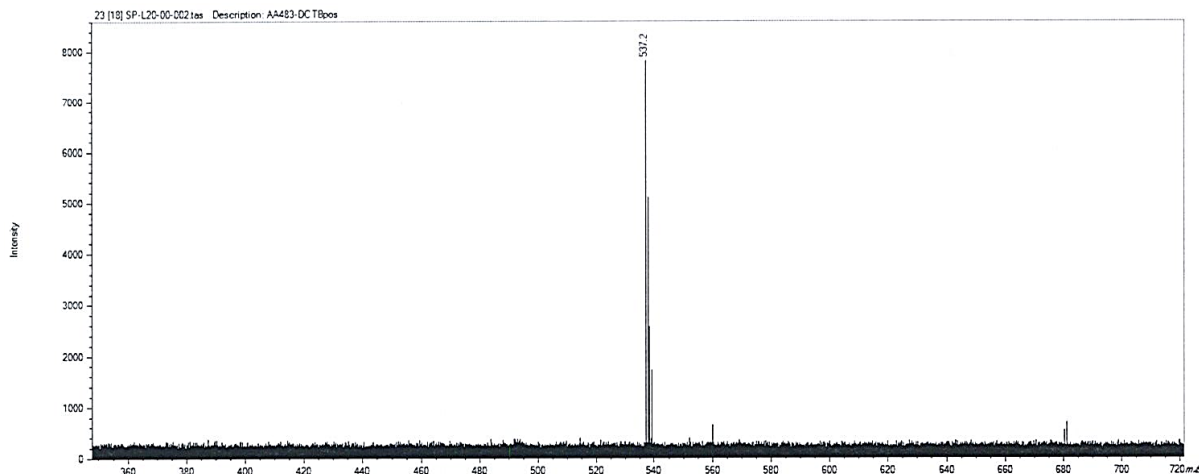


Figure S3. Mass spectrum of 1-bpp[6]helicene.

Chiral HPLC. Analytical chiral HPLC separation for 1-bpp[6]helicene: The sample is dissolved in dichloromethane, injected on the chiral column, and detected with an UV detector at 254 nm and a circular dichroism detector at 254 nm. The flow-rate is 1 mL/min.

Column	Mobile Phase	t ₁	k ₁	t ₂	k ₂	α	R _s
Chiralpak IE	Heptane/2-PrOH/CH ₂ Cl ₂	4.11 (+)	0.39	5.88 (-)	0.99	2.52	8.68

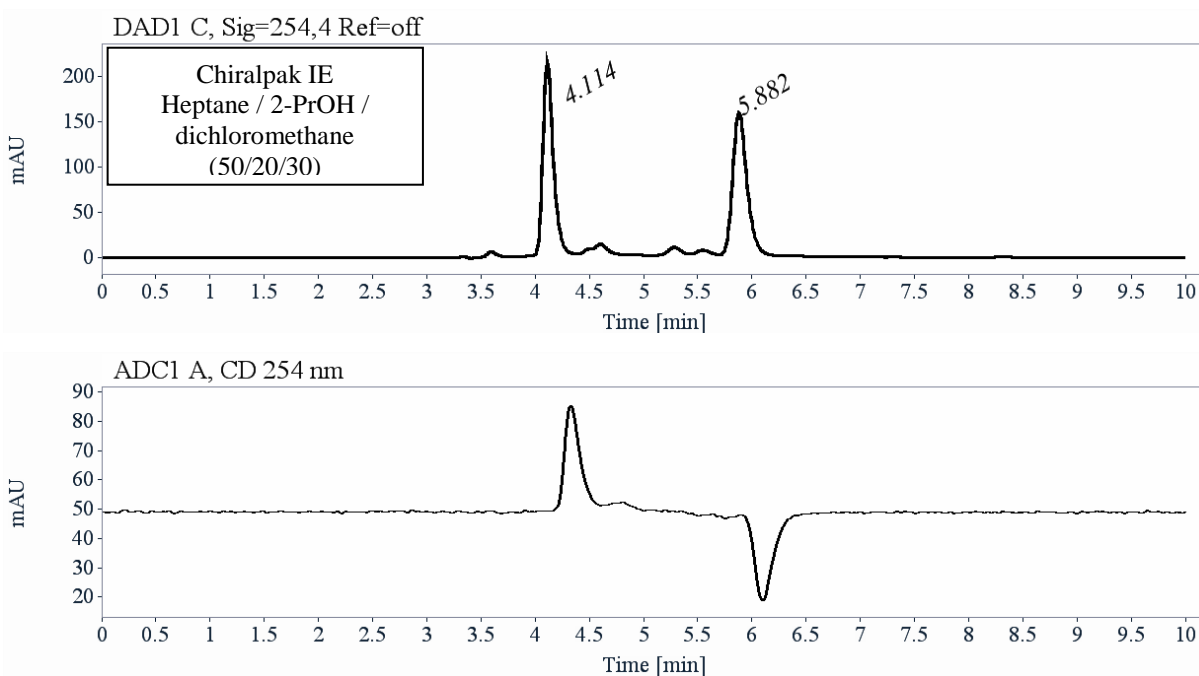


Figure S4. Analytical chiral HPLC separation for 1-bpp[6]helicene.

RT [min]	Area	Area%	Capacity Factor	Enantioselectivity	Resolution (USP)
4.11	1427	49.87	0.39		
5.88	1434	50.13	0.99	2.52	8.68
Sum	2861	100.00			

Preparative separation for 1-bpp[6]helicene:

- Sample preparation: About 135 mg are dissolved in 3 mL of a mixture of CH₂Cl₂ and hexane (67/33).
- Chromatographic conditions: Chiraldak IE (250 x 10 mm), hexane / 2-PrOH / CH₂Cl₂ (50/20/30) as mobile phase, flow-rate = 5 mL/min, UV detection at 254 nm.
- Injections (stacked): 60 times 50 µL, every 5 minutes.
- First fraction: 62 mg of the first eluted enantiomer with ee > 99.5%

RT [min]	Area	Area%
4.11	14615	100.00
Sum	14615	100.00

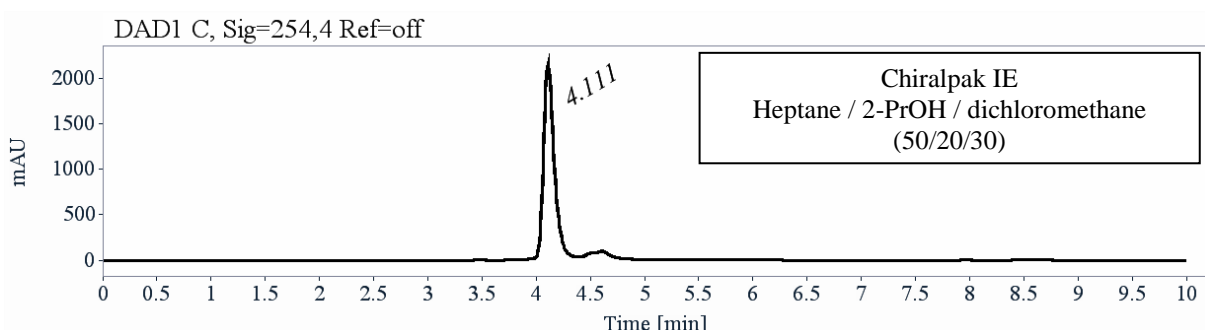


Figure S5. Chiral HPLC separation for 1-bpp[6M]helicene.

- Second fraction: 48 mg of the second eluted enantiomer with ee > 99.5%

RT [min]	Area	Area%
5.97	10402	100.00
Sum	10402	100.00

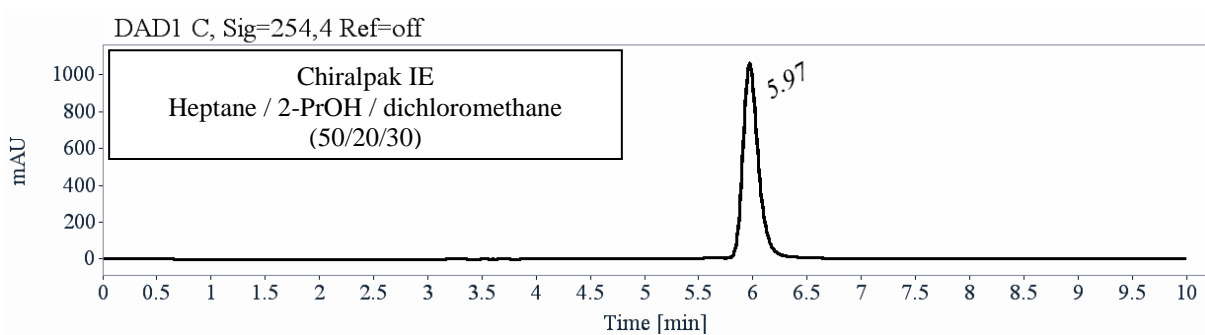


Figure S6. Chiral HPLC separation for 1-bpp[6P]helicene.

Optical rotations: Optical rotations were measured on a Jasco P-2000 polarimeter with a halogen lamp (589 nm, 578 nm, 546 nm and 436 nm), in a 10 cm cell, thermostated at 25°C with a Peltier controlled cell holder.

λ (nm)	1-bpp[6M]helicene first eluted on Chiralpak IE $[\alpha]_D^{25}$ (CH_2Cl_2 , c = 0.057)	1-bpp[6P]helicene second eluted on Chiralpak IE $[\alpha]_D^{25}$ (CH_2Cl_2 , c = 0.062)
589	- 2400	+ 2400
578	- 2550	+ 2550
546	- 3300	+ 3300
436	- 10500	+ 10500

Electronic Circular Dichroism: ECD and UV spectra were measured on a JASCO J-815 spectrometer equipped with a JASCO Peltier cell holder PTC-423 to maintain the temperature at $25.0 \pm 0.2^\circ\text{C}$. A CD quartz cell of 1 mm of optical path length was used. The CD spectrometer was purged with nitrogen before recording each spectrum, which was baseline subtracted. The baseline was always measured for the same solvent and in the same cell as the samples. The spectra are presented without smoothing and further data processing.

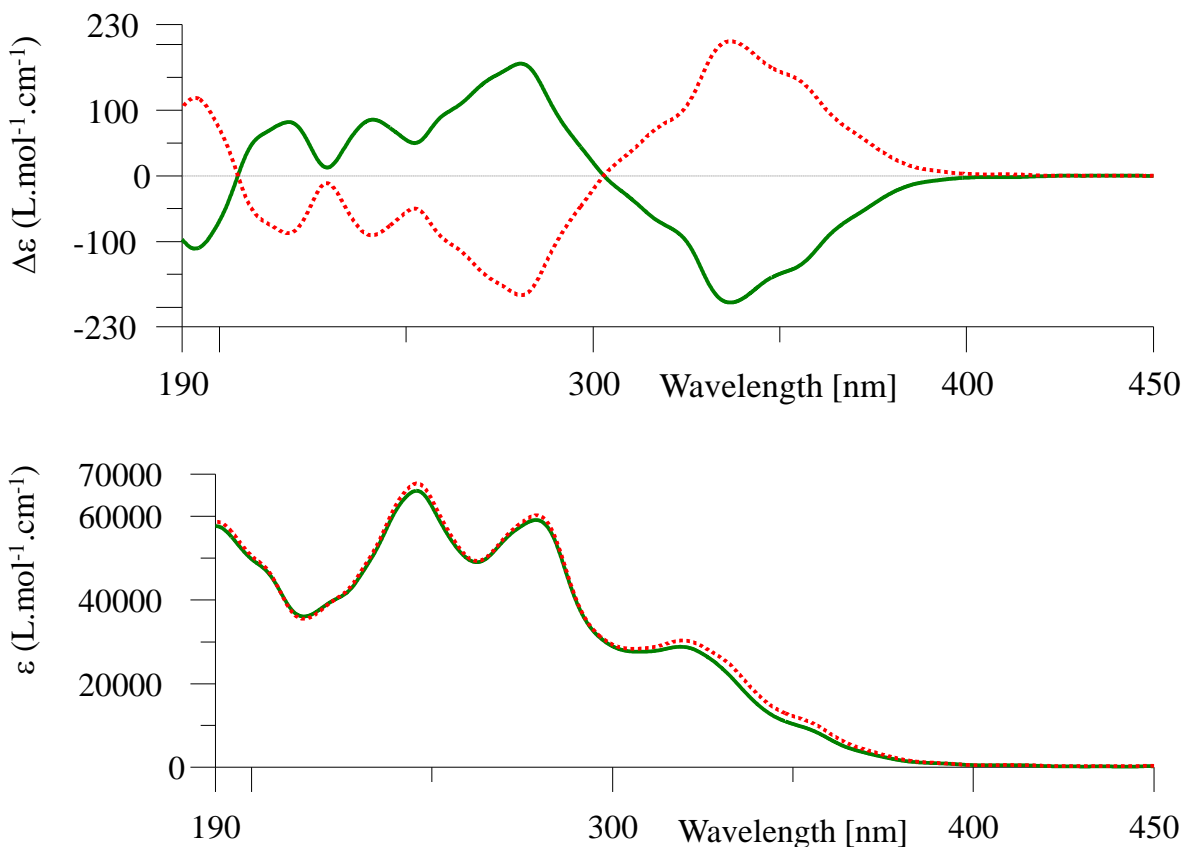


Figure S7. CD (top) and UV-Vis (bottom) spectra for 1-bpp[6M]helicene (green solid line) and 1-bpp[6P]helicene (red dashed line) in acetonitrile solutions at concentrations of $0.240 \text{ mmol}\cdot\text{L}^{-1}$ and $0.248 \text{ mmol}\cdot\text{L}^{-1}$, respectively. Acquisition parameters: 0.1 nm as intervals, scanning speed 50 nm/min, band width 1 nm, and 3 accumulations per sample.

Crystallographic data of the ligands

Table S1. Crystallographic data for **6M** and **6P**.

	6M	6P
Empirical formula	C ₃₇ H ₂₃ N ₅	C ₃₇ H ₂₃ N ₅
Fw	537.60	537.60
Crystal color	Colourless	Colourless
Crystal size (mm ³)	0.40*0.34*0.28	0.12*0.08*0.02
Temperature (K)	150	150
Wavelength (Å)	1.54184	1.54184
Crystal system, Z	Monoclinic, 4	Monoclinic, 4
Space group	P ₂ ₁	P ₂ ₁
a (Å)	9.61830 (10)	9.6325 (2)
b (Å)	14.02930 (10)	14.0237 (2)
c (Å)	20.1535 (2)	20.1322 (3)
α (°)	90	90
β (°)	93.2600 (10)	93.3290 (10)
γ (°)	90	90
V (Å ³)	2715.07 (4)	2714.94 (8)
ρ _{calc} (g.cm ⁻³)	1.315	1.315
μ(CuKα) (mm ⁻¹)	0.620	0.620
θ range (°)	3.841–72.130	3.844–71.988
Data collected	22524	22200
Data unique	10426	10411
Data observed	9924	9833
R(int)	0.0273	0.0280
Nb of parameters / restraints	757/13	757/1
Flack parameter	0.02 (17)	0.18 (16)
R1(F), ^a I > 2σ(I)	0.0334	0.0324
wR2(F ²), ^b all data	0.0890	0.0806
S(F ²), ^c all data	1.046	1.047
CCDC numbers	2101184	2101185

^aR1(F) = Σ|F₀| - |F_C| / Σ|F₀|; ^bwR2(F²) = [Σw(F₀² - F_C²)² / ΣwF₀⁴]^{1/2}; ^cS(F²) = [Σw(F₀² - F_C²)² / (n+r-p)]^{1/2}.

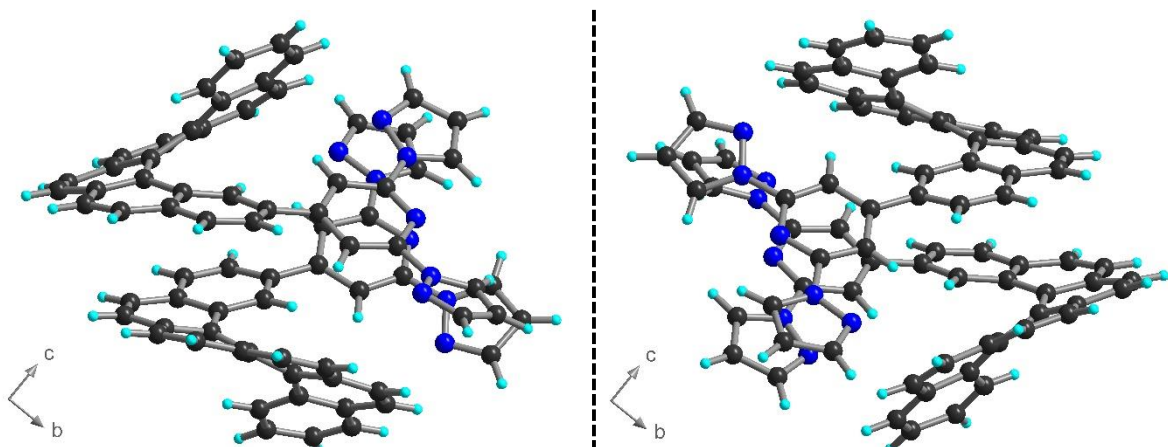


Figure S8. View of the asymmetric unit in **6M** (left) and **6P** (right) along the *a* axis. Color code: C (black), H (cyan), N (blue).

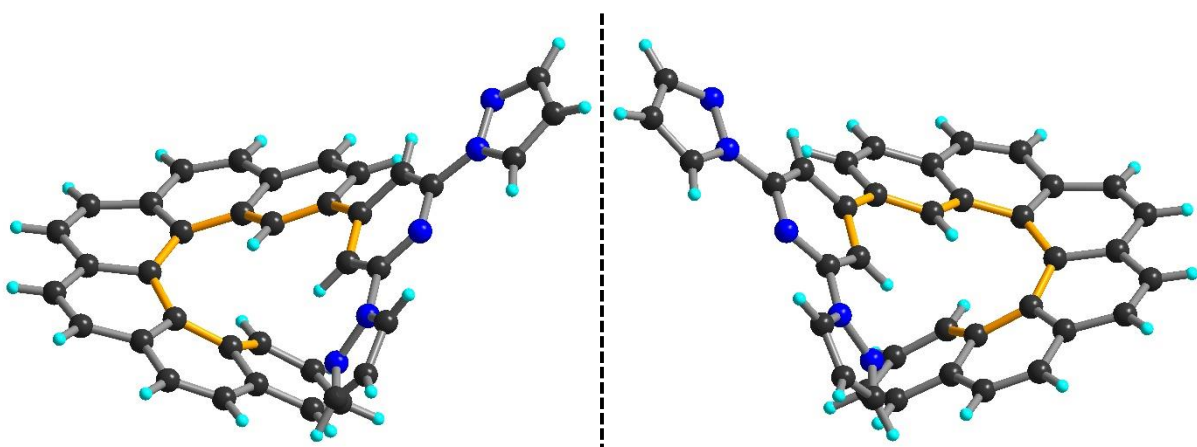


Figure S9. View of the helical curvature of the helicene unit in **6M** (left) and **6P** (right). Selected atom angles reported in Table S2 are highlighted in orange.

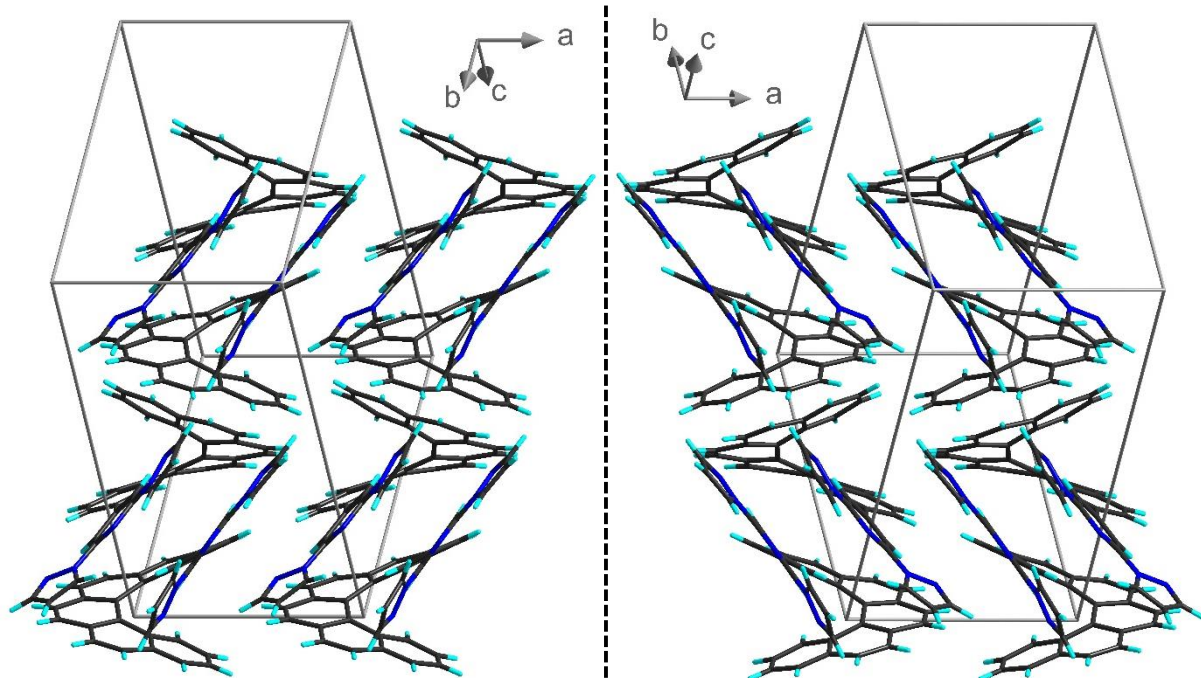


Figure S10. Helicoidal arrangement of the molecules in the crystal packing of **6M** and **6P**. Color code: C (black), H (cyan), N (blue).

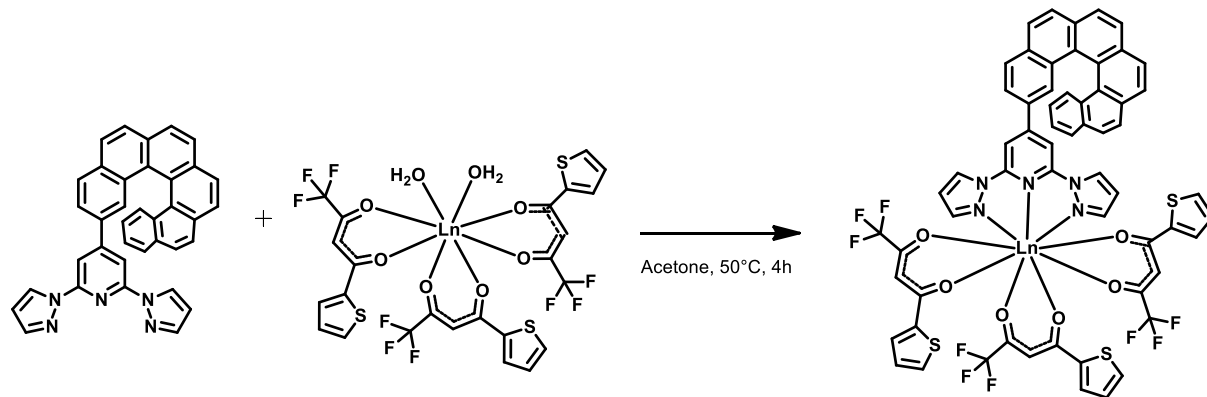
Table S2. Selected bond distances and angles in **6M** and **6P**.

Atoms	Bond distance (Å)	
	6M	6P
C1—C2	1.388(6)	1.388(5)
C2—N1	1.331(4)	1.326(4)
N1—N2	1.352(4)	1.359(3)
N2—C3	1.363(4)	1.362(4)
C3—C1	1.380(5)	1.372(5)
N2—C4	1.416(3)	1.414(3)
C4—C5	1.385(3)	1.384(3)
C5—C6	1.402(3)	1.398(3)
C6—C7	1.398(3)	1.396(3)
C7—C8	1.385(3)	1.386(3)
C8—N3	1.325(3)	1.324(3)
N3—C4	1.330(3)	1.330(3)
C8—N4	1.418(3)	1.420(3)
N4—N5	1.343(3)	1.343(3)
N5—C10	1.329(4)	1.328(4)
C10—C11	1.375(5)	1.380(5)
C11—C9	1.356(5)	1.358(5)
C9—N4	1.358(3)	1.356(3)
C6—C12	1.484(3)	1.487(3)
C12—C13	1.417(3)	1.416(3)
C13—C14	1.362(3)	1.359(3)
C14—C15	1.406(4)	1.406(4)
C15—C16	1.415(3)	1.413(3)
C16—C17	1.419(3)	1.419(3)
C17—C12	1.381(3)	1.381(3)
C15—C18	1.433(3)	1.435(3)
C18—C19	1.340(5)	1.435(3)
C19—C20	1.413(5)	1.414(4)
C20—C21	1.418(4)	1.418(3)
C21—C16	1.466(3)	1.463(3)
C20—C22	1.422(4)	1.422(4)
C22—C23	1.337(5)	1.334(5)
C23—C24	1.414(5)	1.411(5)
C24—C25	1.433(4)	1.433(4)
C25—C21	1.439(4)	1.442(4)
C24—C26	1.399(5)	1.401(5)
C26—C27	1.348(6)	1.350(5)
C27—C28	1.438(5)	1.438(5)
C28—C29	1.407(4)	1.406(4)
C29—C25	1.451(4)	1.451(4)
C28—C30	1.412(5)	1.412(5)
C30—C31	1.346(5)	1.346(5)
C31—C32	1.443(4)	1.438(4)
C32—C33	1.414(4)	1.420(4)
C33—C29	1.452(4)	1.452(4)

C32—C34	1.403(5)	1.405(4)
C35—C36	1.402(4)	1.400(4)
C36—C37	1.372(4)	1.376(3)
C37—C33	1.416(3)	1.416(3)
Atoms		Angle (°)
	6M	6P
C7—C6—C12	121.21(19)	121.11(19)
C6—C12—C17	121.71(19)	121.92(19)
C12—C17—C16	122.3(2)	122.5(2)
C17—C16—C21	123.7(2)	124.1(2)
C16—C21—C25	125.4(2)	125.1(2)
C21—C25—C29	125.6(2)	125.8(2)
C25—C29—C33	124.4(2)	124.3(2)
C29—C33—C37	123.4(2)	123.5(2)

Synthesis and characterization of the complexes [$\text{Ln}(\text{tta})_3(\mathbf{6M})$] and [$\text{Ln}(\text{tta})_3(\mathbf{6P})$].

The ligand enantiomer **6M** or **6P** (0.029 mmol, 15.5 mg) was dissolved in acetone (4 mL) and placed under argon atmosphere. A solution of $[\text{Ln}(\text{tta})_3(\text{H}_2\text{O})_2]$ (0.029 mmol, 25 mg for $\text{Ln} = \text{Eu}$ and 26 mg for $\text{Ln} = \text{Yb}$) in acetone (1 mL) was added and the mixture was stirred at 50°C for 4 hours. The solvent was evaporated under vacuum and the residue was dissolved in a minimum of dichloromethane. Precipitation by addition of *n*-hexane gave the desired product as a yellow powder. Yields: between 56 and 62%.



MALDI: 1130, $[\text{Eu}(\text{tta})_2(\mathbf{6M})]^+$ and $[\text{Eu}(\text{tta})_2(\mathbf{6P})]^+$; 1153, $[\text{Yb}(\text{tta})_2(\mathbf{6M})]^+$ and $[\text{Yb}(\text{tta})_2(\mathbf{6P})]^+$.
Anal. calcd. for $\text{C}_{61}\text{H}_{35}\text{N}_5\text{O}_6\text{S}_3\text{F}_9\text{Eu}$: C, 54.15, H, 2.61, N, 5.18%. Found: C, 54.00, H, 2.48, N, 4.98%. Anal. calcd. for $\text{C}_{61}\text{H}_{35}\text{N}_5\text{O}_6\text{S}_3\text{F}_9\text{Yb}$: C, 53.32, H, 2.57, N, 5.10%. Found: C, 53.05, H, 2.39, N, 4.85%.

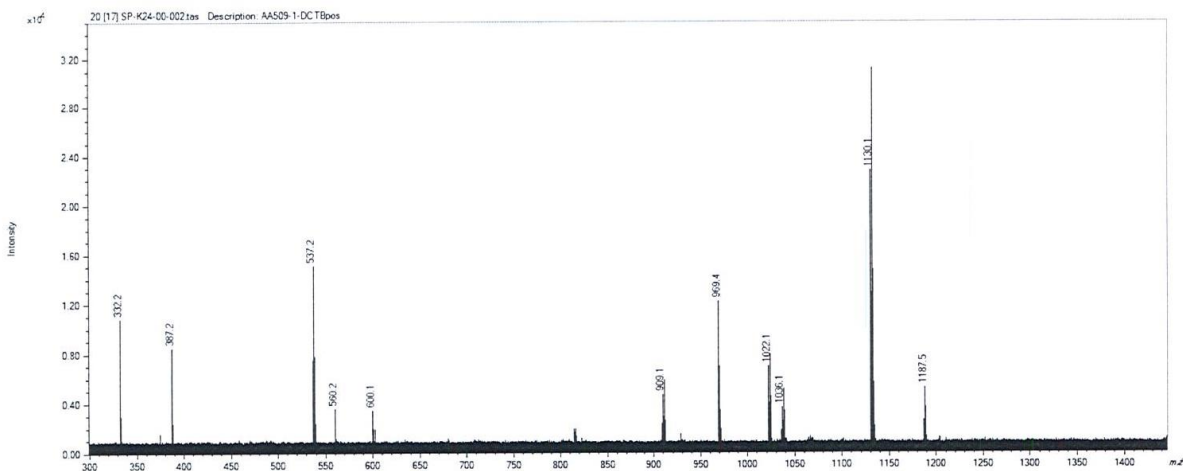


Figure S11. Mass spectrum of $[\text{Eu}(\text{tta})_3(\mathbf{6M})]$.

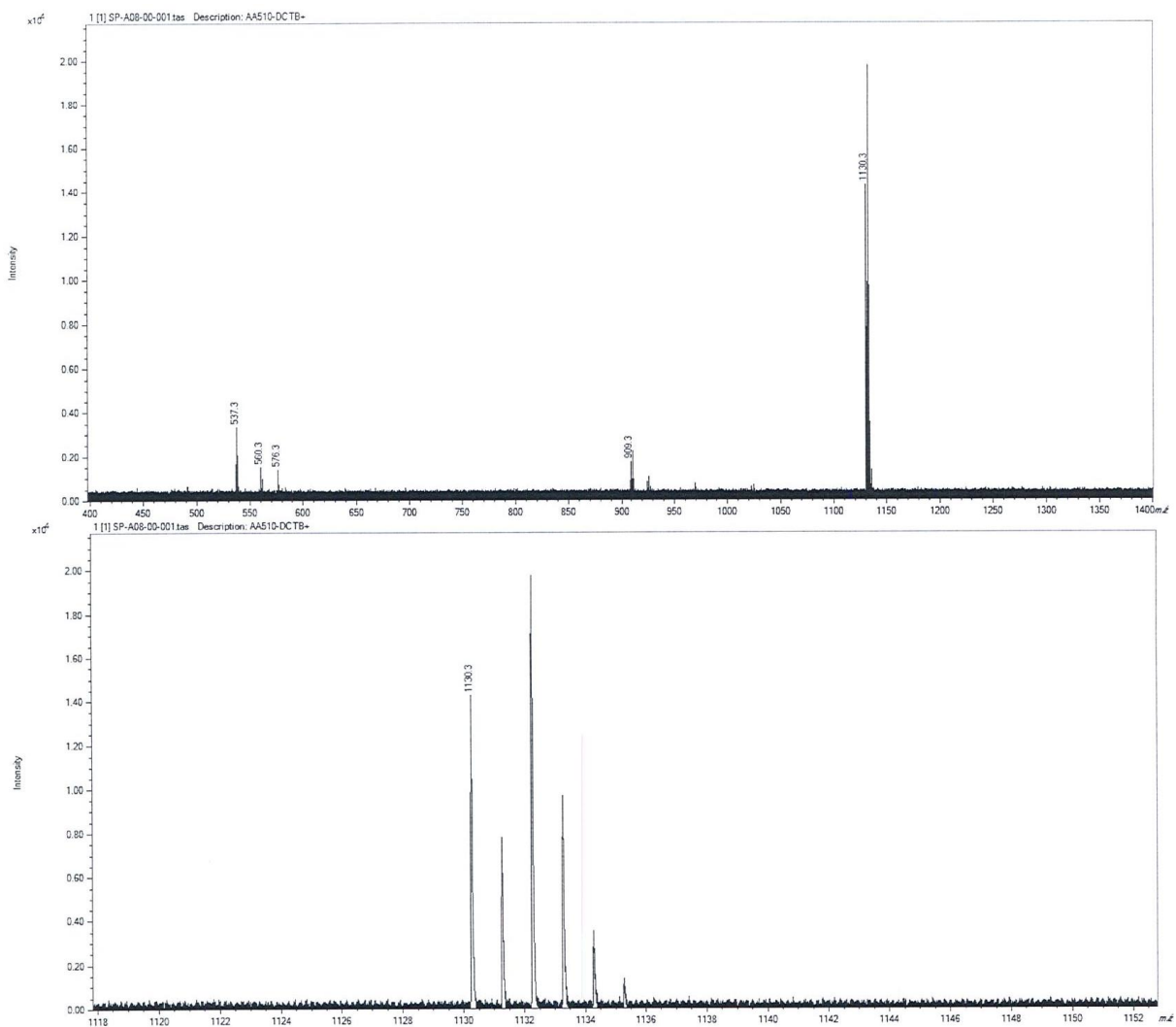


Figure S12. Mass spectrum of $[\text{Eu}(\text{tta})_3(\mathbf{6P})]$.

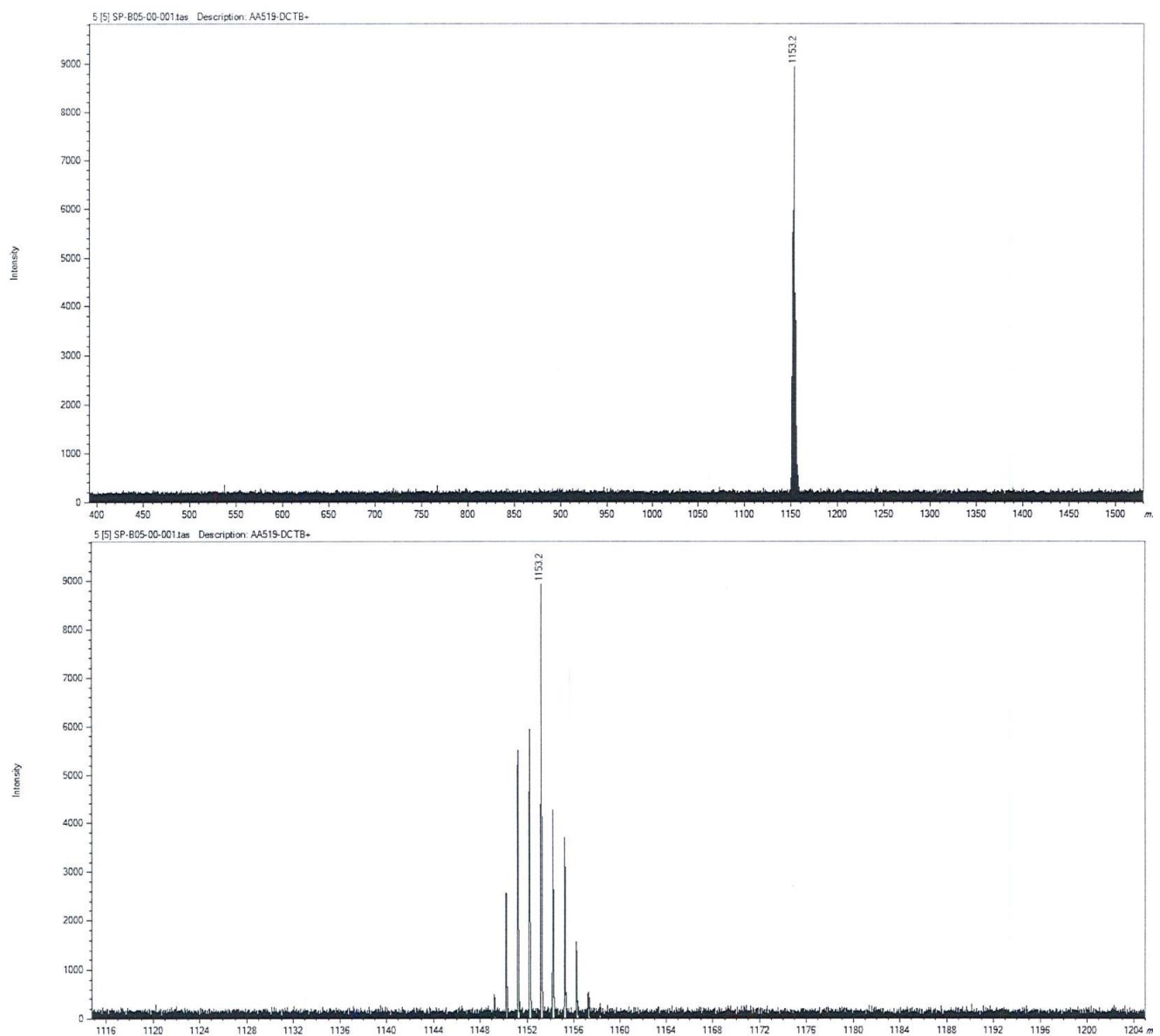


Figure S13. Mass spectrum of $[Yb(tta)_3(6M)]$.

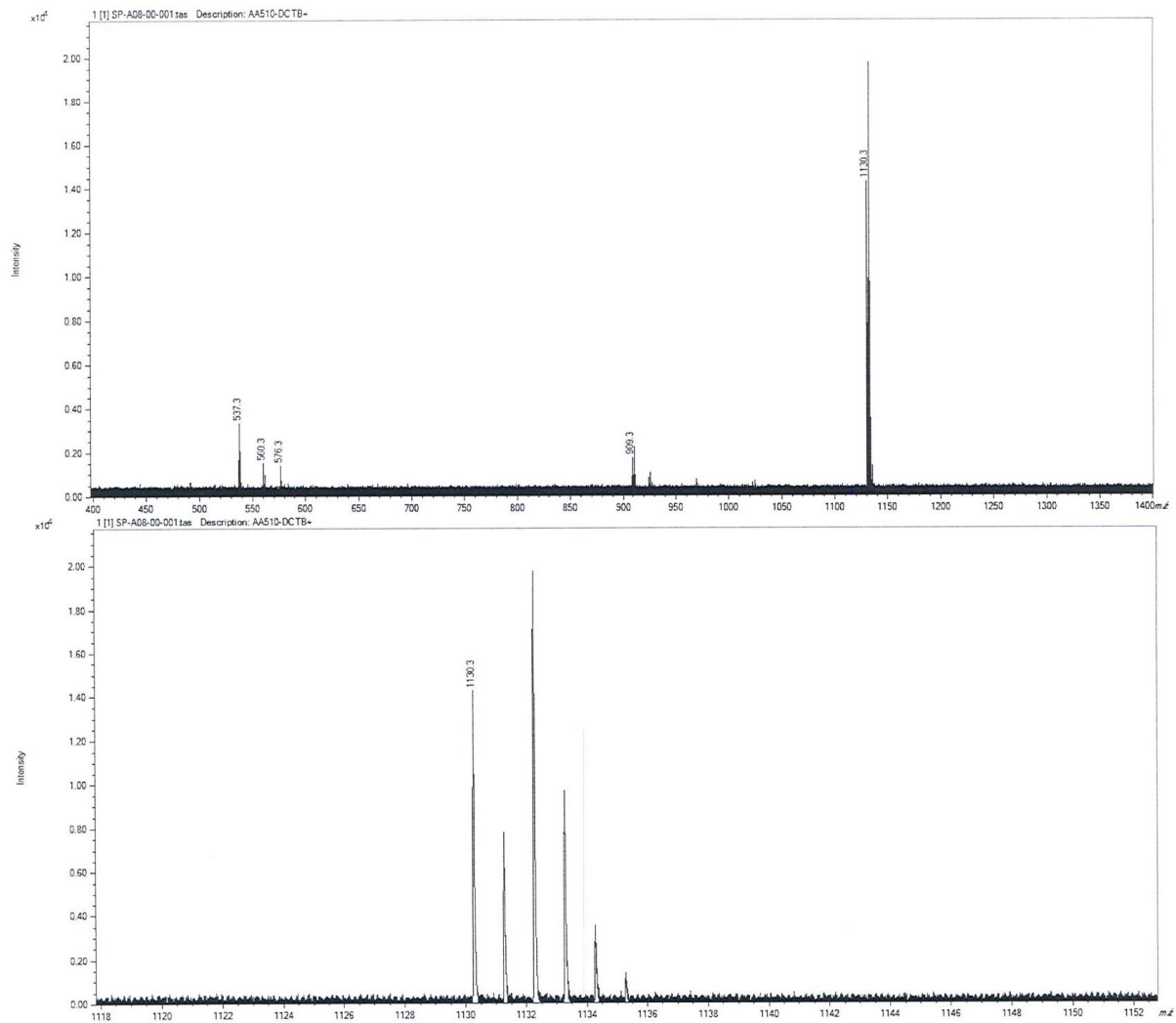


Figure S14. Mass spectrum of $[Yb(tta)_3(6P)]$.

UV-Vis / CD spectroscopy of the complexes

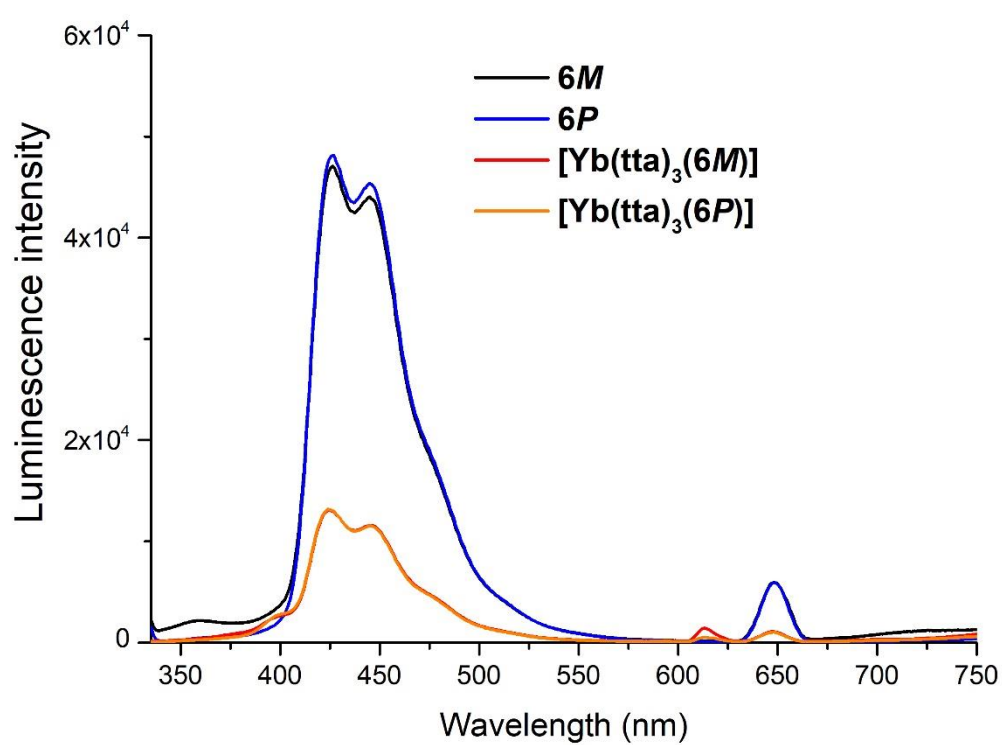
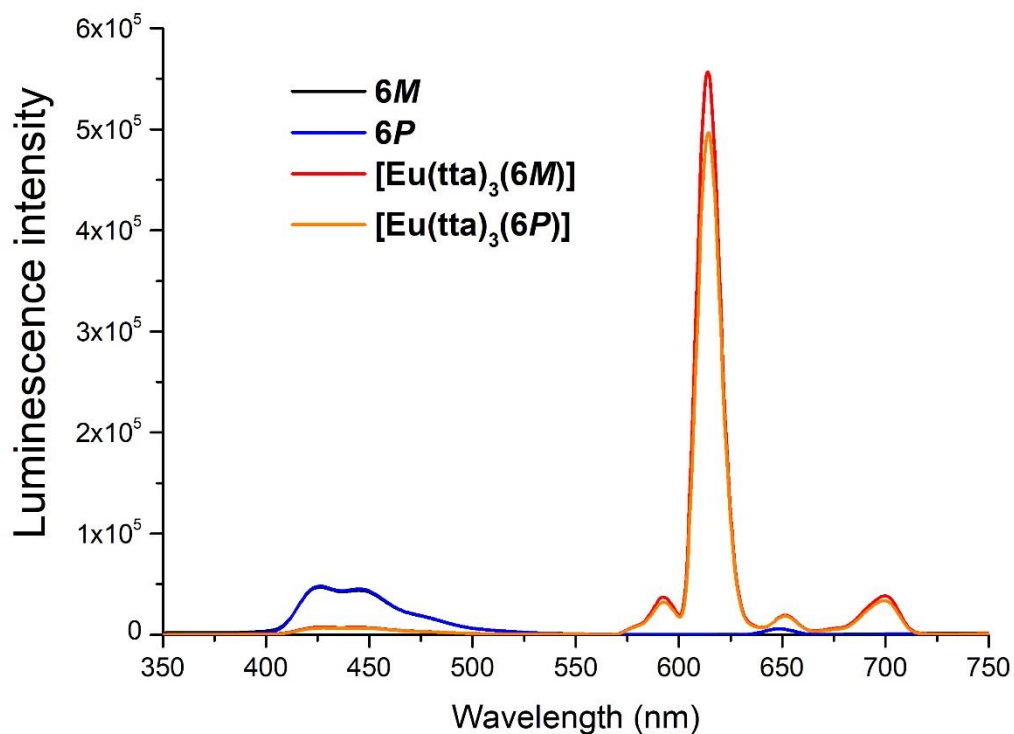


Figure S15. Emission spectra for ligands and complexes in 10^{-6} M CH_2Cl_2 solutions. Excitation wavelength: 325 nm.

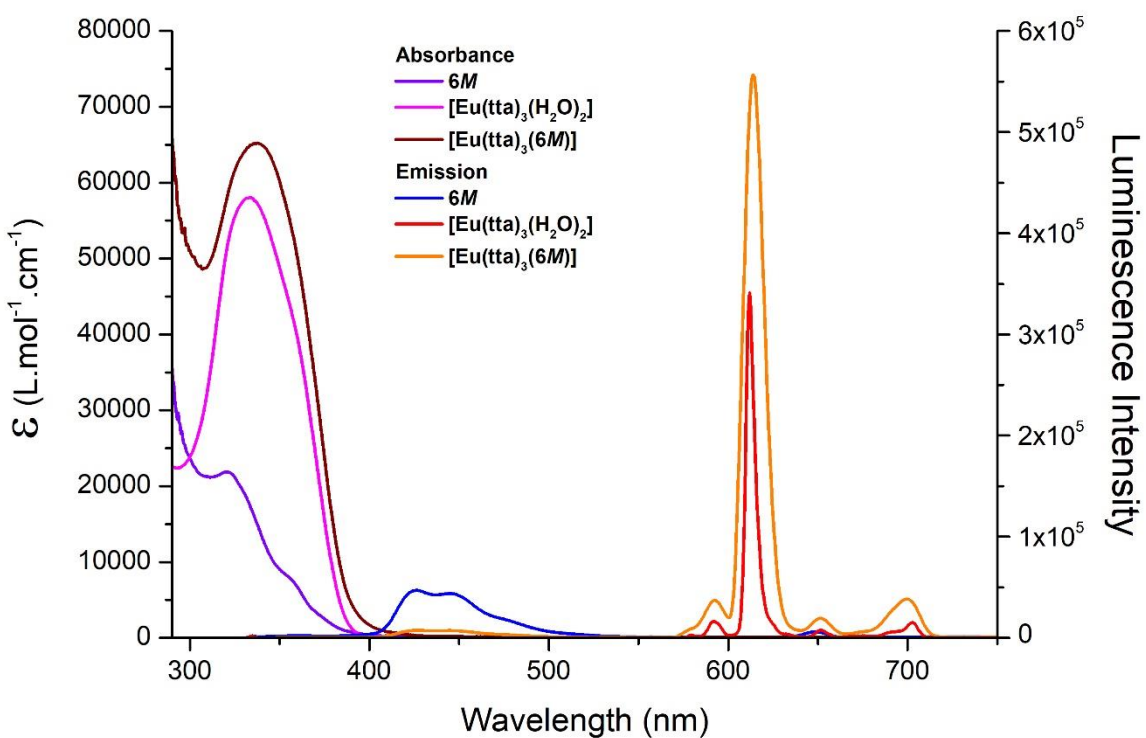


Figure S16. UV-Vis absorbance and emission spectra for **6M**, $[\text{Eu}(\text{tta})_3(\text{H}_2\text{O})_2]$ and $[\text{Eu}(\text{tta})_3(\mathbf{6M})]$. Excitation wavelength for emission measurement: 325 nm.

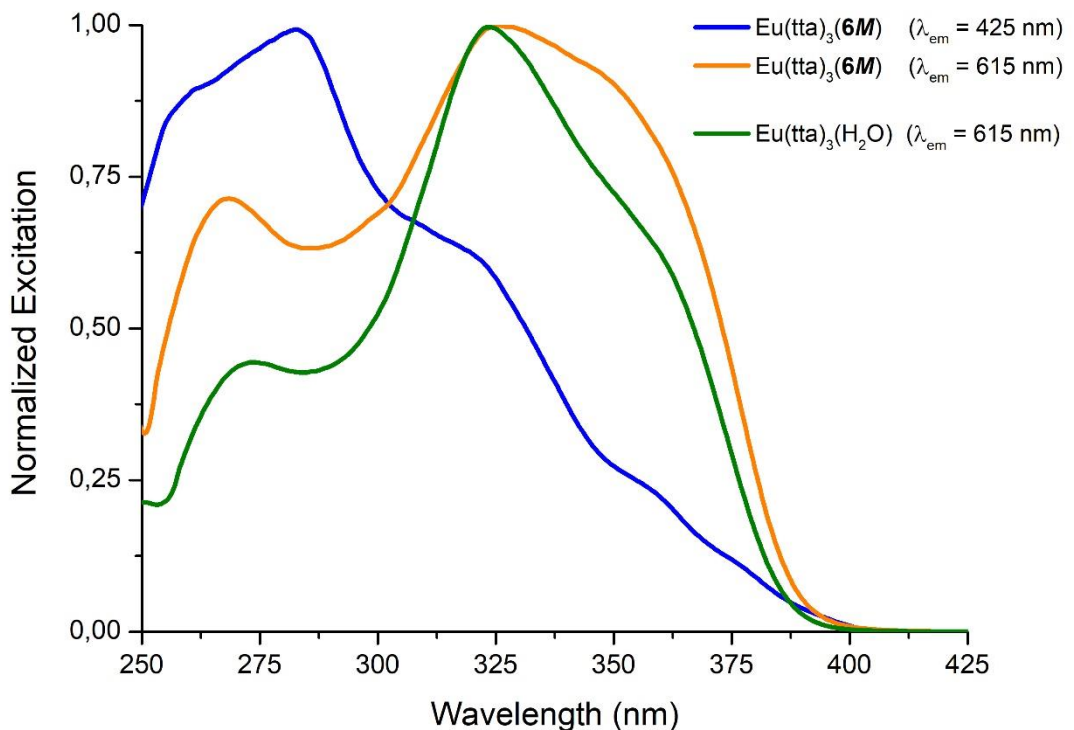


Figure S17. Normalized excitation spectra for $[\text{Eu}(\text{tta})_3(\text{H}_2\text{O})_2]$ and $[\text{Eu}(\text{tta})_3(\mathbf{6M})]$.

CPL of the complexes

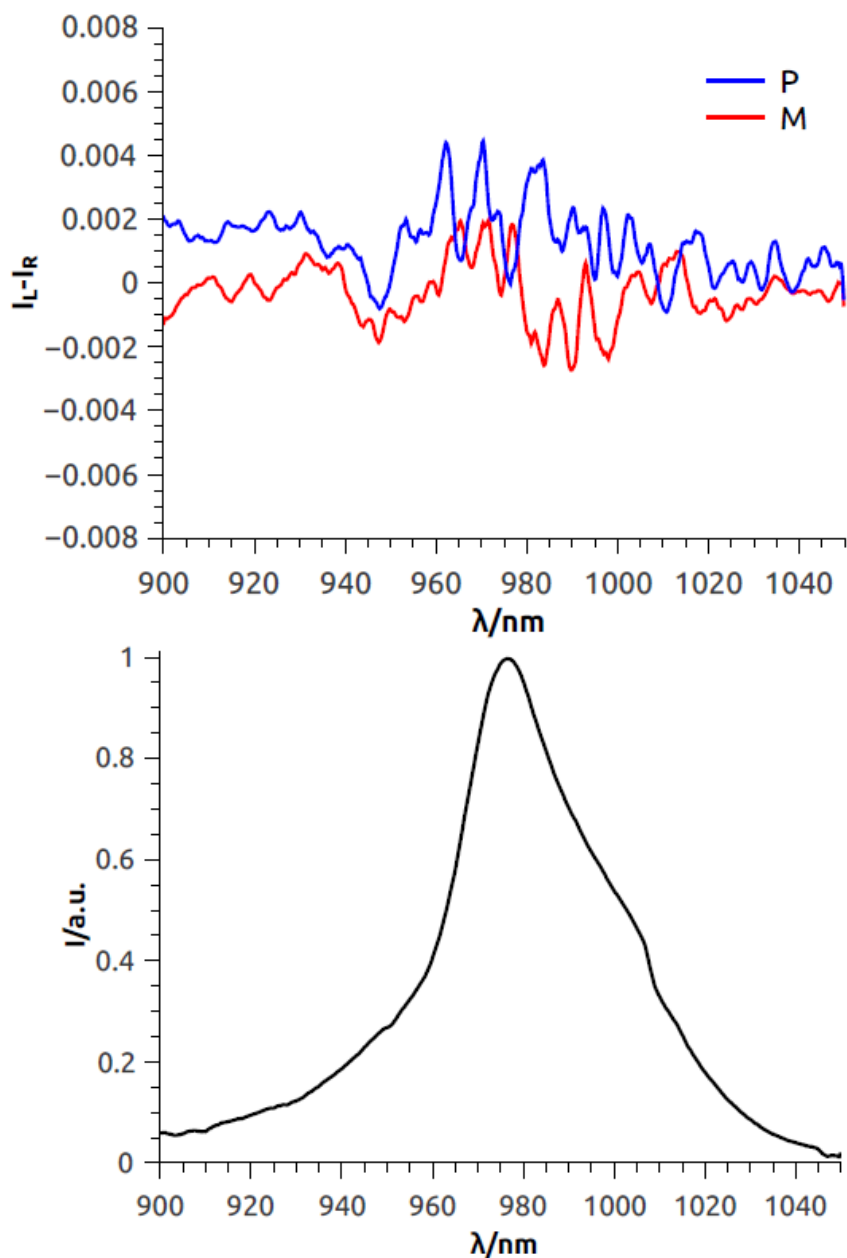


Figure S18. CPL and emission spectra of dichloromethane solutions of $[\text{Yb}(\text{tta})_3(\mathbf{6M})]$ and $[\text{Yb}(\text{tta})_3(\mathbf{6P})]$ in the NIR region.

Additional calculated data.

Table S3. Computed TDA TDDFT data for selected dominant excitations of the **6M** ligand.

Excitation	E (eV)	λ (nm)	length-gauge		velocity-gauge	
			f (a.u.)	$R \cdot 10^{-40}$ (esu ² cm ²)	f (a.u.)	$R \cdot 10^{-40}$ (esu ² cm ²)
# 1	3.26	380	0.02	-47	0.01	-28
# 2	3.40	365	0.21	-681	0.13	-443
# 3	3.56	348	0.29	-910	0.16	-558
# 4	3.67	338	0.30	236	0.11	139
# 6	3.95	314	0.22	-231	0.09	-120
# 7	3.96	313	0.27	160	0.10	121
# 9	4.07	305	0.95	747	0.39	403
# 15	4.39	282	0.30	117	0.12	-22
# 21	4.72	263	0.62	117	0.33	119
# 22	4.78	259	0.29	-120	0.09	-47
# 24	4.84	256	0.68	47	0.23	15
# 25	4.88	254	0.05	-102	0.02	-72
# 27	4.95	251	0.09	103	0.04	84
# 32	5.06	245	0.30	129	0.14	89
# 33	5.19	239	0.32	96	0.19	83
# 34	5.20	238	0.13	-91	0.08	-141
# 38	5.32	233	0.25	-250	0.12	-129
# 41	5.37	231	0.30	51	0.17	8

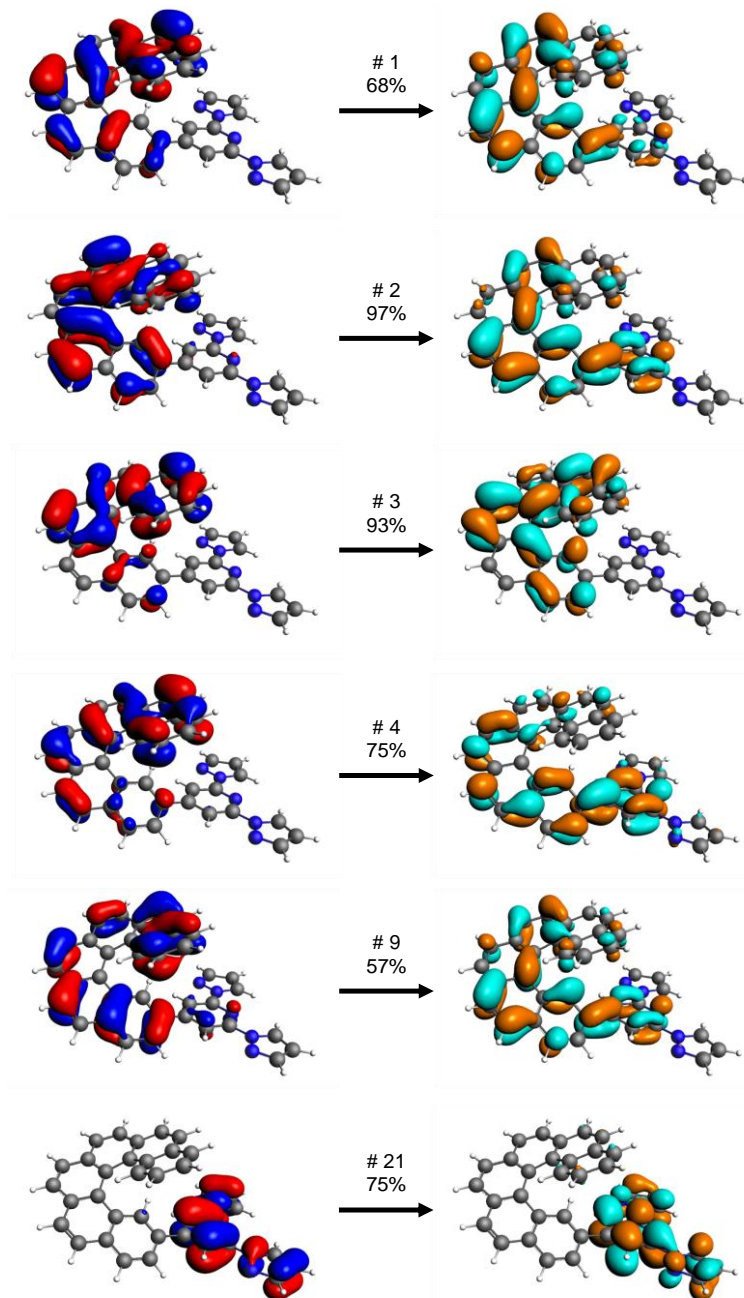


Figure S19. Isosurfaces (± 0.03 a.u.) of NTOs involved in selected transitions of **6M**. Hashtag values refer to the numbering of the depicted excitation. Percentage values refer to the contribution of the printed couple of NTO in the description of the transition.

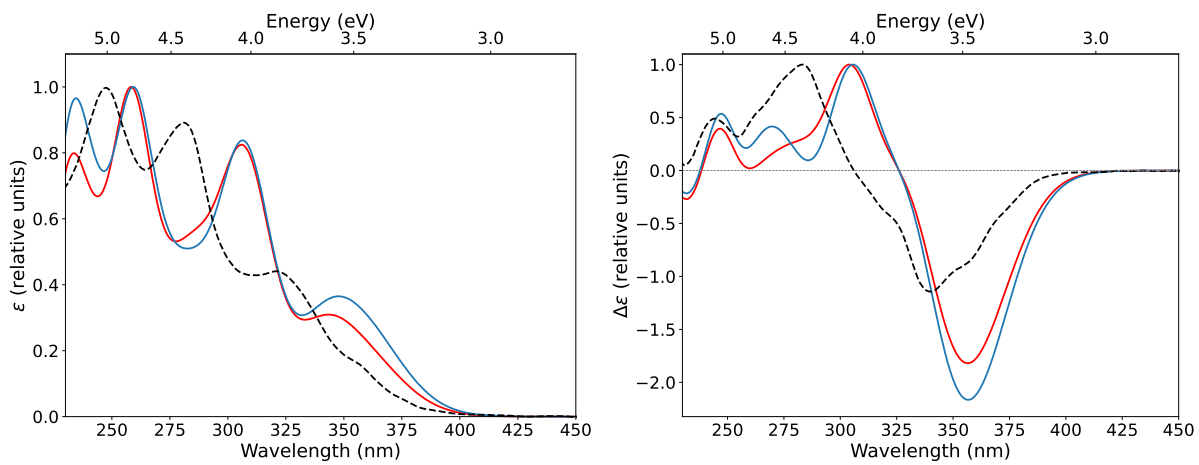


Figure S20. Comparison between the TDA TDDFT simulated UV-Vis (left) and CD (right) spectra of **6M** ligand using the length-gauge formalism (red line) and the velocity-gauge formalism (blue line) in relative units. Experimental spectra are plotted in black dashed lines.

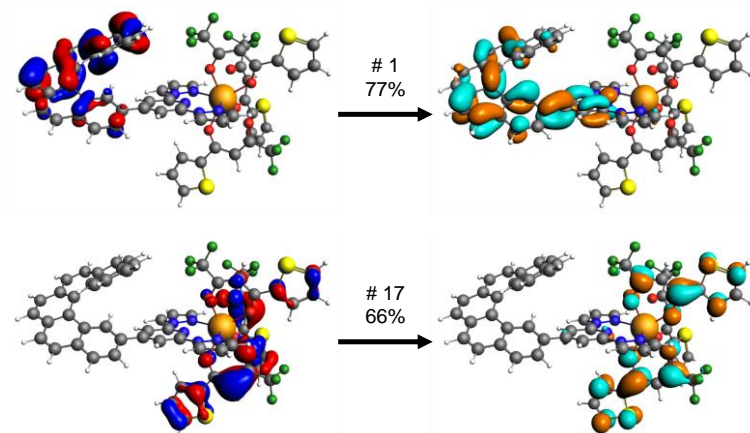


Figure S21. Isosurfaces (± 0.03 a.u.) of NTOs involved in selected transitions of $[Y(tta)_3(6M)]$ complex. Hashtag values refer to the numbering of the depicted excitation. Percentage values refer to the contribution of the printed couple of NTO in the description of the transition.

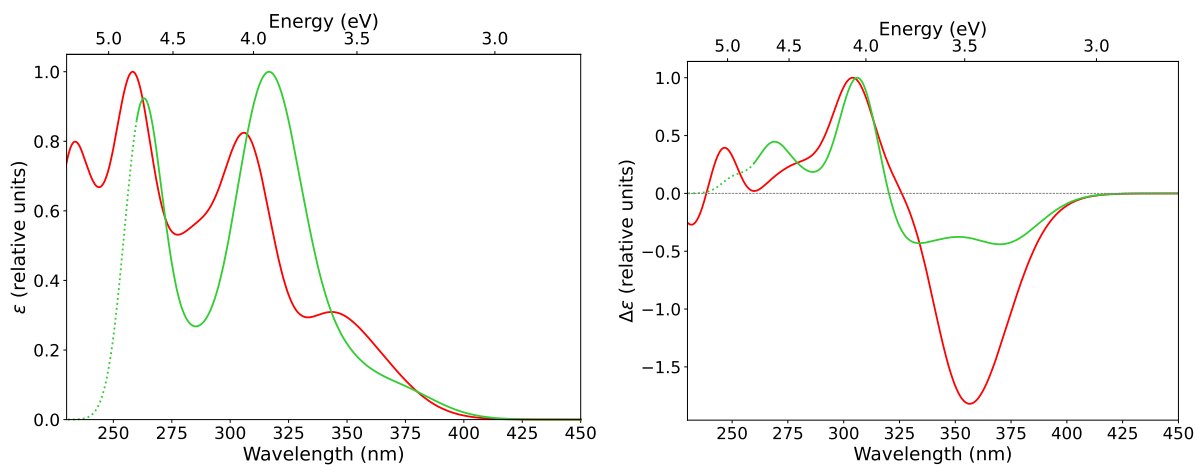


Figure S22. Comparison between the TDA TDDFT simulated UV-Vis (left) and CD (right) spectra of **6M** ligand (red line) and $[Y(tta)_3(\mathbf{6M})]$ complex (green line) in relative units. The spectra of the $[Y(tta)_3(\mathbf{6M})]$ complex are dotted under 260 nm because there is not enough calculated excitation energies in order to correctly reproduce the shape.

Table S4. Energetic mean of first spectroscopic levels of the $[Eu(tta)_3(\mathbf{6M})]$ complex from CAS(6,7)SCF calculations.

$^{2S+1}L_J$ level	E mean (cm^{-1})
5D_3	28 010
5D_2	24 913
5D_1	22 347
5D_0	20 677
7F_6	5 390
7F_5	4 182
7F_4	3 026
7F_3	1 974
7F_2	1 071
7F_1	384
7F_0	0

Table S5. Energetic splitting of the $[Yb(tta)_3(\mathbf{6M})]$ complex from CAS(13,7)SCF calculations. KD stands for Kramer's doublets.

$^{2S+1}L_J$ level	E of KD (cm^{-1})	E mean (cm^{-1})
	10 601	
$^7F_{5/2}$	10 392	10 439
	10 324	
	337	
	202	
$^7F_{7/2}$	55	149
	0	

Table S6. SOC calculated as root mean squares in cm^{-1} between the five first excited singlet and triplet states of **6M** at the optimized geometry of S_0 (left table) and S_1 (right table).

$\langle S H_{\text{SOC}} T \rangle$	T ₁	T ₂	T ₃	T ₄	T ₅	$\langle S H_{\text{SOC}} T \rangle$	T ₁	T ₂	T ₃	T ₄	T ₅
S ₁	0.74	0.17	0.22	0.10	0.31	S ₁	0.74	0.18	0.19	0.05	0.39
S ₂	0.14	0.34	0.52	0.50	0.37	S ₂	0.14	0.44	0.73	0.35	0.39
S ₃	0.20	0.37	0.61	0.48	0.23	S ₃	0.13	0.27	0.36	0.83	0.07
S ₄	0.26	0.65	0.19	0.34	0.24	S ₄	0.44	0.77	0.47	0.24	0.16
S ₅	0.37	0.10	0.19	0.19	0.35	S ₅	0.33	0.10	0.28	0.24	0.29

Table S7. Computed data of the CPL from $^5\text{D}_0$ excited state to all multiplets lower in energy than 5 000 cm^{-1} for the [Eu(tta)₃(**6M**)] complex from CAS(6,7)SCF calculations.

Transition	E (eV)	E (cm^{-1})	λ (nm)	R ($\text{esu}^2 \text{cm}^2$)	f_{ED} (a.u.)	f_{MD} (a.u.)
$^7\text{F}_5 \leftarrow ^5\text{D}_0$	2.032	16 388	610	8.95E-47	2.20E-13	5.73E-12
	2.033	16 400	610	-2.65E-46	1.01E-11	1.05E-12
	2.035	16 413	609	1.34E-46	1.30E-11	9.12E-13
	2.037	16 426	609	7.86E-47	5.19E-13	1.35E-12
	2.039	16 442	608	1.67E-46	5.52E-12	5.33E-13
	2.047	16 508	606	4.22E-47	1.63E-12	1.16E-13
	2.050	16 538	605	-3.10E-48	1.98E-12	3.37E-13
	2.052	16 554	604	-8.24E-48	1.59E-12	4.81E-14
	2.054	16 569	604	-7.18E-48	8.76E-13	5.06E-13
	2.059	16 604	602	4.30E-48	3.40E-13	1.77E-13
	2.059	16 611	602	-9.84E-48	7.62E-13	2.51E-13
$^7\text{F}_4 \leftarrow ^5\text{D}_0$	2.171	17 514	571	1.72E-45	2.42E-10	1.24E-12
	2.177	17 556	570	5.00E-46	3.19E-10	2.85E-12
	2.186	17 629	567	-7.60E-46	5.76E-10	1.58E-11
	2.188	17 650	567	-3.01E-45	1.18E-09	3.11E-12
	2.190	17 666	566	-1.71E-46	2.60E-10	6.72E-13
	2.191	17 674	566	1.41E-45	8.20E-10	4.29E-12
	2.194	17 693	565	-4.76E-47	1.15E-11	1.78E-13
	2.196	17 709	565	1.13E-45	1.35E-10	8.08E-12
	2.203	17 769	563	-8.32E-47	1.46E-10	1.09E-13
	2.313	18 659	536	6.73E-47	1.41E-12	8.62E-13
$^7\text{F}_3 \leftarrow ^5\text{D}_0$	2.315	18 672	536	-7.92E-46	3.08E-12	6.83E-11
	2.316	18 678	535	-5.35E-47	2.76E-12	3.90E-11
	2.318	18 699	535	1.63E-45	7.27E-12	4.54E-11
	2.321	18 719	534	1.90E-46	2.23E-12	1.30E-11
	2.323	18 738	534	-7.29E-46	3.97E-12	2.92E-11
	2.326	18 757	533	-3.05E-47	1.53E-12	1.41E-11
$^7\text{F}_2 \leftarrow ^5\text{D}_0$	2.423	19 542	512	2.14E-45	2.96E-10	3.07E-12

	2.425	19 556	511	-4.19E-45	1.79E-10	4.70E-11
	2.431	19 609	510	5.15E-45	6.12E-10	1.47E-10
	2.433	19 626	510	1.97E-45	1.75E-10	2.57E-11
	2.442	19 698	508	-4.53E-45	1.34E-09	9.58E-12
	2.504	20 198	495	3.31E-45	1.26E-12	2.25E-08
$^7F_1 \leftarrow ^5D_0$	2.519	20 316	492	-2.61E-46	1.95E-12	2.25E-08
	2.525	20 365	491	-4.32E-45	6.79E-13	2.27E-08
$^7F_0 \leftarrow ^5D_0$	2.564	20 677	484	3.41E-47	3.72E-09	8.32E-17

¹ A. I. Voloshin, N. M. Shavaleev, V. P. Kazakov, *J. Lumin.* **2000**, *91*, 49–58.

² M. Jakubec, T. Beránek, P. Jakubík, J. Sýkora, J. Žádný, V. Církva, J. Storch, *J. Org. Chem.* **2018**, *83*, 3607–3616.

³ F. Zinna, T. Bruhn, C. A. Guido, J. Ahrens, M. Bröring, L. Di Bari, G. Pescitelli, *Chem. Eur. J.* **2016**, *22*, 16089–16098.

⁴ F. Zinna, L. Arrico, L. Di Bari, *Chem. Commun.* **2019**, *55*, 6607–6609.

⁵ A. Abhervé, K. Martin, A. Hauser, N. Avarvari, *Eur. J. Inorg. Chem.* **2019**, 4807–4814.